Characterization of Polymer Thin Films with Small-Angle X-ray Scattering under Grazing Incidence (GISAXS)

DETLEF-M. SMILGIES
CHESS G-line Division, Cornell University, Ithaca, NY 14853, USA

PETER BUSCH AND CHRISTINE M. PAPADAKIS
Faculty of Physics and Earth Sciences, University of Leipzig, Linnéstr. 5, D-04103 Leipzig, Germany

DORTHE POSSELT
Dept. of Mathematics and Physics (IMFUFA), Roskilde University, DK-4000 Roskilde, Denmark

Polymer thin films have numerous technical applications as functional coatings, the most prominent example being PMMA coatings for lithography of integrated circuits and micromechanical devices. Polymer blends and block copolymers can be tailored for specific mechanical, optical, electric, and chemical properties. For instance, functional surfaces have been created by means of polymer blend and diblock copolymer films that may serve as templates for nanolithography [1] or as antireflection coatings [2]. In the rapidly developing field of molecular electronics, opto-electronical properties of polymer films have been exploited and first devices have appeared on the market [3].

The structure and properties of block copolymers in thin film geometry can be significantly different from the bulk. The presence of two interfaces, the air-film interface and the film-substrate interface, can induce preferential ordering in the films, in particular if the film thickness is on the order of the typical length scale of the block copolymer microstructure [4,5]. For thin films two interfacial contributions to the free energy have been identified: the interface energies of each component favoring the component with the lowest interfacial energy to accumulate at the interface, as well as chain stretching parallel to the interface reducing the interface entropy of the blocks, which may promote a perpendicular orientation of the lamellar interfaces with respect to the walls. In Monte Carlo simulations of symmetric diblock copolymers, which form a lamellar phase in the bulk, it was shown that the lamellae orient parallel to the interface, if the interfacial energies of the blocks differ considerably, whereas for similar interfacial energies of the blocks a perpendicular orientation of the lamellae with respect to the interface is favorable [6]. Experimental studies varying the interface selectivity in a systematic way have been reported [7].

Another effect coming into play is the commensurability of the lamella period with the film thickness, which again can either favor a parallel (commensurate) or perpendicular (incommensurate) orientation [8]. For polymer films with a free surface, it has frequently been found that the film has two distinct thicknesses: islands or holes are formed in the upper layers with a step height corresponding to one lamellar thickness [9].

The classic tool in studying the structure of block copolymer thin films is transmission electron microscopy (TEM) [10]. This technique provides detailed local information on the microstructure, but is very demanding in sample preparation. The perpendicular density profile of thin films has traditionally been studied with X-ray reflectivity (XR) [11], with some spectacular results on the PS-PMMA block copolymer system, where the PMMA block strongly favors absorption on the polar silicon oxide layer of a silicon wafer, leading to a parallel lamellar orientation [5]. An important technique for imaging the surface structure of block copolymer thin films is atomic force microscopy (AFM) in tapping mode [1,12]. In order to overcome the problem of its exclusive surface sensitivity, AFM has been combined with reactive ion etching [13], so that details of the interior film structure could be identified locally. In our studies, we have chosen to combine surface imaging by AFM with a technique that does not lead to destruction of the sample and, moreover, provides accurately averaged information about a large sample area: grazing-incidence small-angle X-ray scattering (GISAXS).

Why did we choose the grazing-incidence geometry? Typical and technically interesting substrates like silicon wafers or glass have thicknesses on the order of 1 mm and would require rather hard X-ray beams for a transmission experiment. Furthermore, the weak scattering from a film of typically 200 Å to 2000 Å thickness can be obscured by scattering from the substrate, whereas in grazing-incidence geometry the penetration of the X-ray photons into the substrate is limited when the angle of incidence is close to the critical angle. GISAXS was first applied to the problem of nanoparticles on solid surfaces by Levine et al. [14] and Naudon et al. [15]. There is currently strong interest in the technique

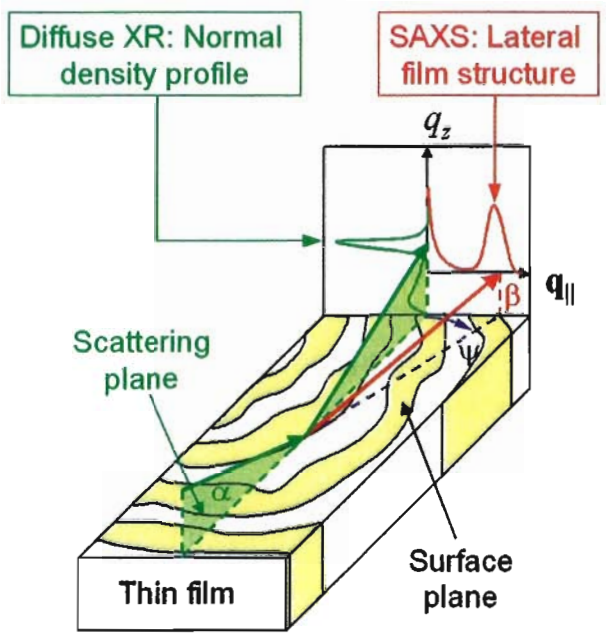

Figure 1: GISAXS scattering geometry: incident angle α, in-plane scattering angle ψ, and exit angle β. The cut of the incident plane with the area detector corresponds to a detector scan in diffuse reflectivity. Lateral structure in the film gives rise to SAXS-like scattering parallel to the sample surface. Line scans corresponding to these two special situations are indicated as the red and green curves. The penetration of the X-ray beam into the film is controlled by choosing appropriate incident angles close to the critical angle.

for studying morphology and self-organization at solid surfaces during growth and ion erosion [16], as well as characterizing the shape functions and correlations of quantum dot arrays [17]. Earlier applications to polymer films addressed the questions of dewetting and roughness correlations between the substrate and the polymer film [18]. Finally, the scattering theory is described within the framework of distorted-wave Born approximation [19].

The information contained in a GISAXS intensity map is shown schematically in Figure 1. We distinguish between the scattering parallel and perpendicular to the sample surface, as indicated by the respective components of the scattering vector $\mathbf{q}_{||}$ and q_z. The intensity in the incident plane is determined by the specular and diffuse reflectivity [19], with diffuse Bragg sheets extending out into the $q_{||}$ direction which provide information on the perpendicular density profile of the film. Parallel to the surface small-angle scattering features can appear indicating lateral ordering in the film. The scattering can be rod-like, such as the scattering rods in grazing-incidence diffraction [20], or display scattering rings, as in transmission SAXS. Since both the reflectivity signal and the small-angle scattering signal fall off with q^{-4} according to the laws of Fresnel and Porod, it is advantageous to measure the weak scattering signals at low incident angles close to the critical angle, as long as the film is still fully penetrated by the X-ray wave.

CHESS D-line

Scattering experiments were performed at CHESS D-line. D-line is located on a hard-bent dipole magnet of the CESR storage ring and uses a W:C multilayer monochromator with about 1.5 percent band path providing 10^{12} photons per mm^2 and sec at a photon energy of 8 keV. Two collimation slits and a guard slit condition the beam before it impinges onto the sample surface. With a typical sample footprint along the beam of 40 mm and an incident angle around 0.2°, the sample accepts about 100 μm of beam vertically. In order to prevent diffuse scattering due to beam overspill, the vertical width was further reduced to 50 μm. A 1.25 mm molybdenum rod mounted at a distance of about 1 m from the sample served as a beam stop for the direct beam of a horizontal width of 0.5 mm as well as for the intense reflected beam and the diffuse scattering in the incident plane. The described set-up is able to resolve structures up to of 1000 Å in size.

Custom-built fiber-optically coupled CCD cameras [21] were used for the detection of the scattering intensity. Pixel sizes were 50.8 μm and 80 μm, respectively, with image sizes of 1024 x 1024 pixels in both cases. The dynamic range of these detectors extends from about 10 to 50,000 counts per pixel, and is well adjusted to the rapidly decaying scattering intensity. Exposure times are controlled by a fast shutter in the incident beam. The detector is protected by a secondary slow shutter during line-up. The outside of the slow shutter is coated with a large area photocell, which was used to position the beam stop properly in the direct and reflected beams. Furthermore, we could use the photocell to position the sample into the beam and to detect the reflected beam from the sample in order to identify scattering angles slightly above the critical angle.

The sample cell, shown in Figure 2, consists of a base plate to which the samples could be clamped with soft leaf spring and a cover with 8 μm Kapton windows. A reservoir in the sample cell below the sample holder could be used to expose the samples to solvent vapor. The solvent could be injected into the cell with a syringe and a long Teflon capillary tube from outside the hutch. A small light bulb mounted on the top lid of the cell prevented condensation of the solvent on the sample surface and the windows by raising their respective temperatures by a couple of degrees above ambient. The cell was mounted on a goniometer controlling the incident angle and the sideways tilt of the sample. The sample

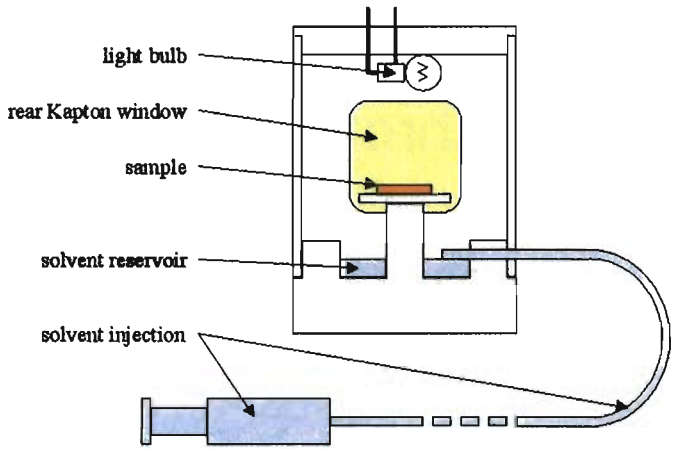

Figure 2: Cross section through the sample cell used for vapor treatment of polymer thin films, viewed in beam direction. The X-ray beam enters and exits the cell through thin Kapton windows. Toluene liquid can be injected into a reservoir below the sample from outside the hutch via a long Teflon tube. In order to avoid cross-linking due to radiation damage, which would affect the dynamics of the film, the cell can be shifted laterally through the beam for successive exposures. A small light bulb mounted on the top of the cell provides a small amount of heating to prevent condensation of solvent vapor on the sample and on the windows.

could be centered accurately in the beam with a height translation. Moreover, in order to control radiation damage on the films, the cell could be shifted laterally to expose fresh parts of the sample to the beam. This way, up to 30 pristine spots could be examined on a single sample.

Samples were prepared by spin coating of polymer solution onto silicon wafers. Toluene was used as a close-to non-selective solvent for symmetric polystyrene-polybutadiene (PS-PB) diblock copolymers of molecular weights between 13.9 and 183 kg/mol. In earlier experiments, we observed a previously unpredicted molar mass dependence of the film morphology [22]. Low-molar mass films (13.9–69.9 kg/mol) preferred a parallel ordering of the lamellae, whereas lamellae of high-molar mass films (91.9–183 kg/mol) ordered perpendicular to the substrate, as evident from the surface texture AFM image in Figure 3a and the Bragg rods in the GISAXS map (Figure 3b).

In order to investigate the stability of such films, we exposed a high molar mass film (183 kg/mol) to solvent vapor. With 10 sec exposures and about 20 sec read-out time we could follow morphology changes in the film on a time scale of minutes. We observed changes in the scattering intensity during half an hour after injection of the solvent into the cell [23]. Before solvent exposure, the GISAXS map was characterized by scattering rods with a $q_{\|}$-vector close to the bulk lamella period, indicating a perpendicular orientation of the lamellae (see Figure 3b). After solvent exposure these scattering rods curved inwards to form a partial ring (Figure 4a), which indicates that there were undulations of the lamellar interfaces. Hence exposure to solvent vapor induces a tran-

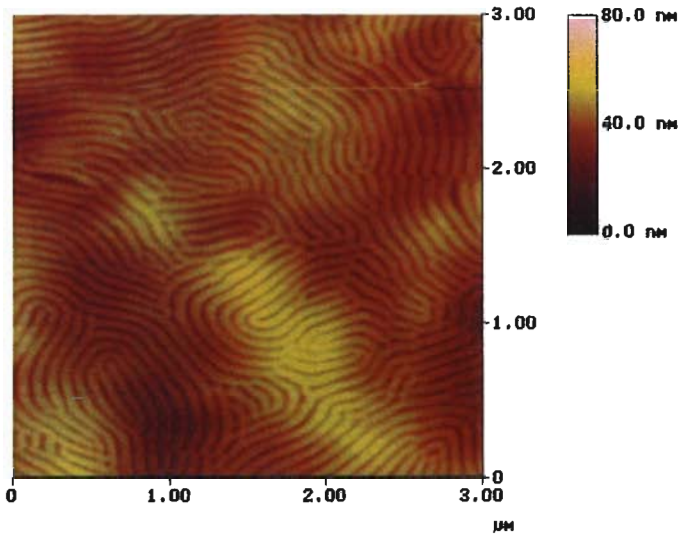

(a)

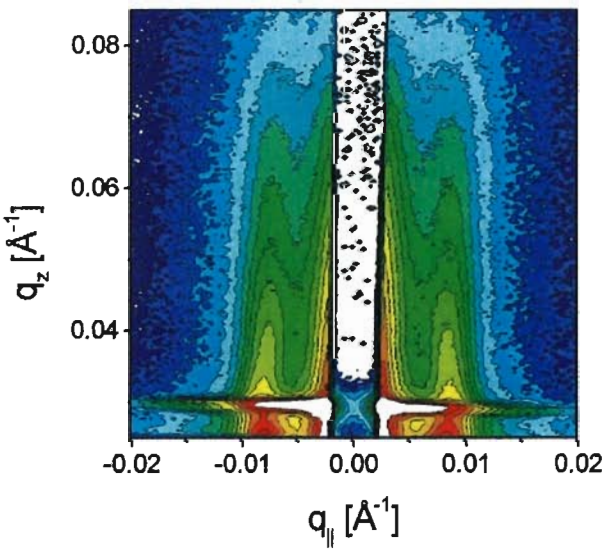

(b)

Figure 3: A thin PS-PB film with a molar mass of 183 kg/mol, bulk lamellar period of 839 ± 13 Å, and a film thickness of 2320 Å. (a) Tapping mode AFM height image. Image size is size 3 μm x 3 μm. The vertical scale between darkest and lightest parts of the image corresponds to 80 nm. (b) GISAXS intensity map on a logarithmic scale with the minimum and maximum values corresponding to 25 and 5,000 counts per pixel. The incident angle was 0.20° at a photon energy of 8 keV. The vertical stripe down the middle of the GISAXS pattern is the shadow of the beamstop. Straight Bragg rods at $q_{||}$ of 0.008 Å^{-1} indicate the formation of perpendicular lamellae.

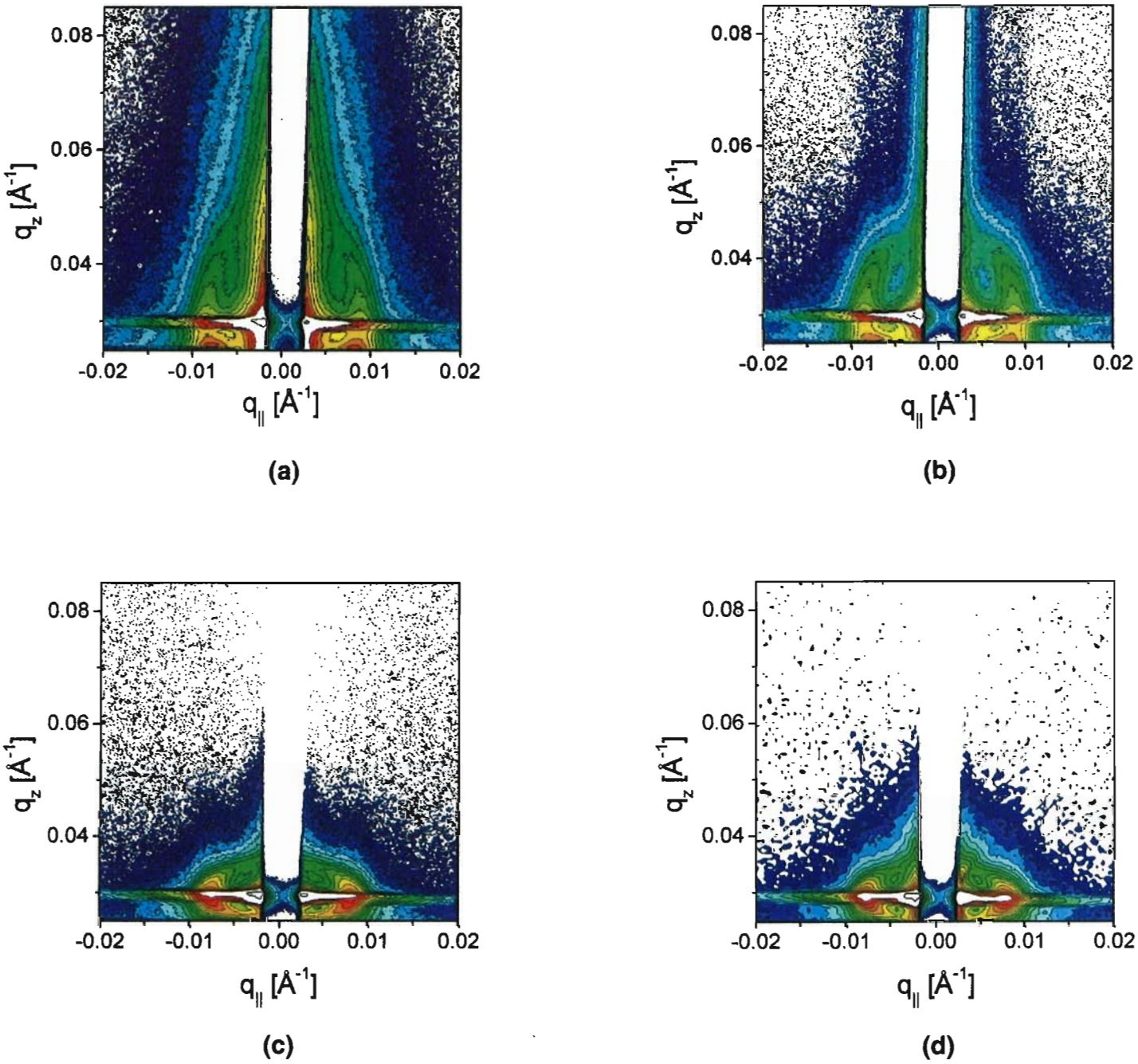

Figure 4: Time-evolution of the GISAXS pattern of the sample shown in Figure 3 during exposure to toluene vapor. (a) 1 min, (b) 4 min, (c) 17 min, and (d) 33 min, after toluene injection into the sample chamber. Already after 1 min of exposure, the rods start to curve, indicative of tilting of the lamellae upon solvent uptake. After 17 min the film is fully swollen to about twice its initial thickness, as estimated from the decrease of the extend of the Bragg rod. After 33 min no more significant changes are observed; the film appears to have taken up the equilibrium toluene concentration at ambient temperature.

sition from a 2D powder (lamellar domains with a preferential orientation perpendicular to the surface) to a more bulk-like 3D powder (lamellar domains with arbitrary orientation) on as short a time scale as minutes. Moreover, the spread of the scattering intensity perpendicular to the surface was reduced showing the swelling of the polymer film (Figure 4c,d). Surprisingly, when the solvent vapor was removed the scattering revealed again 2D-like scattering rods, i.e. the transformation was at least partially reversible. Hence the investigated films seem to form relatively stable structures despite the strong non-equilibrium character of the spin-coating process.

Conclusion

In summary, we have shown that the GISAXS technique can be exploited to investigate the lateral structure of polymer thin films on a mesoscopic length scale of up to ~1000 Å. A variety of film morphologies were observed for symmetric diblock copolymers of different molecular weights. The GISAXS scattering signal is sufficiently strong to permit studies of the film dynamics on a time scale of minutes. Basic scattering features are visible in the CCD detector images even within exposure times of seconds. Hence, a time-scale of seconds seems accessible by optimizing the detection scheme. A GISAXS set-up is being included in the new ultra-high flux CHESS G1 station presently under construction. ■

Acknowledgements

We thank Sol Gruner for stimulating discussions and commenting on the manuscript. Special thanks to Ernie Fontes for setting up CHESS D-line and Mark Tate for help with the 2D detectors. Thanks also to Oleg Konovalov and Gerhard Grübel at the ESRF Troika beamlines, where complementary experiments were performed. CHESS is a NSF and NIH/NIGMS funded national research laboratory under award DMR 9713424. G-line is funded under NSF grant DMR-9970838. We acknowledge further funding by Deutsche Forschungsgemeinschaft, NATO Collaborative Linkage Grant No. 978046, and Fonds der Chemischen Industrie.

References

1. J. Spatz et al., *Adv. Mater.* **10,** 849 (1998); T. Thurn-Albrecht et al., *Science* **290,** 2126 (2000).
2. S. Walheim et al., *Science* **283,** 520 (1999).

3. Z. Bao et al., *MRS Bulletin* **27,** 441 (2002).
4. E. Huang et al., *Macromolecules* **32,** 5299 (1999); M. J. Fasolka et al., *Macromolecules* **33,** 5702 (2000); M. J. Fasolka and A. M. Mayes, *Ann. Rev. Mater. Res.* **31,** 323 (2001).
5. S. H. Anastasiadis et al., *Phys. Rev. Lett.* **62,** 1852 (1989); S. H. Anastasiadis et al., *J. Chem. Phys.* **92,** 5677 (1990); A. Menelle et al., *Phys. Rev. Lett.* **68,** 67 (1992).
6. J.-U. Sommer, A. Hoffmann, and A. Blumen, *J. Chem. Phys.* **111,** 3728 (1999).
7. G. J. Kellogg et al., *Phys. Rev. Lett.* **76,** 2503 (1996); E. Huang et al., *Macromolecules* **33,** 80 (2000).
8. T. Geisinger, M. Müller and K. Binder, *J. Chem. Phys.* **111,** 5241 (1999).
9. G. Coulon, D. Ausserre and T. P. Russell, *J. Phys. France* **51,** 777 (1990); Z.-H. Cai et al., *J. Chem. Phys.* **98,** 2376 (1993).
10. H. Hasegawa and T. Hashimoto, *Macromolecules* **18,** 589 (1985); A. Turturro et al., *Polymer* **36,** 3987 (1995); G. Kim and M. Libera, *Macromolecules* **31,** 2569 (1998).
11. T. P. Russell, *Materials Science Reports* **5,** 171 (1990).
12. D. Schwark et al., *J. Mater. Sci. Lett.* **11,** 352 (1992); S. N. Magonov et al., *Surface Science* **389,** 201 (1997); D. N. Leonard et al., *Macromolecules Rapid Commun.* **23,** 205 (2002).
13. C. Harrison et al., *Macromolecules* **31,** 2185 (1998); R. Magerle, *Phys. Rev. Lett.* **85,** 2749 (2000).
14. J. Levine et al., *J. Appl. Cryst.* **22,** 528 (1989).
15. A. Naudon in H. Brumberger (ed.), *Modern Aspects of Small-Angle Scattering,* (Kluwer Academic Publishers, Amsterdam, 1995) p. 181.
16. M. V. Ramana Murty, *Surf. Sci.* **500,** 523 (2002).
17. T. H. Metzger et al., *Thin Solid Films* **336,** 1–8 (1998).
18. P. Müller-Buschbaum and M. Stamm, *Macromolecules* **31,** 3686 (1998); J. S. Gutmann et al., *Physica B* **283,** 40 (2000).
19. S. K. Sinha et al., *Phys. Rev. B* **38,** 2297 (1988); M. Rauscher, T. Salditt, and H. Spohn, *Phys. Rev. B* **52,** 16855 (1995).
20. J. Als-Nielsen and D. McMorrow, *Elements of Modern X-ray Physics* (John Wiley and Sons, New York, 2001).
21. M. W. Tate et al., *J. Appl. Cryst.* **28,** 196 (1995); D.J. Thiel et al., *Rev. Sci. Instr.* **67,** 1 (1996).
22. P. Busch, D. Posselt, D.-M. Smilgies, and C. M. Papadakis, submitted.
23. P. Busch, D. Posselt, D.-M. Smilgies, and C. M. Papadakis, unpublished.